A R C H I V E S O F M E T A L L U R G Y A N D M A T E R I A L S
Volume 53 2008 Issue 3

J. DIONIZAK*

ON NUMERICAL ANALYSIS OF THERMAL RADIATION IN PARTICIPATING AND SCATTERING MEDIUM IN METALLURGICAL FURNACES

ANALIZA NUMERYCZNA RADIACYJNEJ WYMIANY CIEPŁA W PIECACH METALURGICZNYCH W OBECNOŚCI ZAWIESINY PYŁÓW

There are numerous examples of metallurgical processes, when the technological process involves single or multiphase reacting flow at high temperature. The influence of thermal radiation on physical and chemical processes must be accounted for when reliable process modeling results are expected. Thermal radiation calculation can be cumbersome if inadequate numerical method is applied. The paper presents the thermal radiation model for the mixed convection, conduction and radiation heat transfer with participating media. The flux and discrete ordinates methods has been used for the solution of some example problems. Finally, the model application in 3D flash smelting process simulation has been discussed, where multiphase reacting flow is strongly influenced by the thermal radiation. The obtained results shows the dominant role of radiation scattering and emission of solid/liquid particles in overall heat transfer in the flash smelter. It is strongly advised to close the heat transfer problem by the auxiliary calculation of heat losses through the furnace walls, as it removes necessity to supply assumed temperatures of the walls and stabilizes numerical computations. Simulation results were compared with available industrial measurements.

Keywords: metallurgical process simulation, radiation heat transfer, numerical methods, flash smelting

Wielofazowy przepływ z reakcjami chemicznymi w wysokich temperaturach występuje w wielu procesach metalurgicznych. Wpływ promieniowania cieplnego na przebieg konwersji chemicznej i fizycznej musi być uwzględniony na tyle precyzyjnie aby możliwe było uzyskanie wartościowych wyników symulacji takich procesów. Obliczenia wymiany ciepła przez promieniowanie może być bardzo pracochłonne o ile zostanie dobrana niewłaściwa metoda numeryczna. W artykule przedstawiono model radiacyjnego transportu energii dla mieszanej konwekcyjno-dyfuzyjnej i promienistej wymiany ciepła w ośrodku rozpraszająco-emitującym. Model oparto na równaniu transportu energii promienistej. Opisano zastosowanie metod numerycznych strumieni i kierunków dyskretnych na paru prostych przykładach. Przedstawiono także implementację opisanych metod do 3-wymiarowej symulacji procesu zawiesinowego wytopu miedzi. Otrzymane wyniki ujawniają dominującą rolę zjawiska rozpraszania i emisji promieniowania przez cząstki koncentratu w procesie wymiany ciepła w piecu zawiesinowym. Zaleca się domknięcie modelu transportu ciepła przez dodatkowe obliczenia strat ciepła przez ściany pieca, dzięki czemu unika się konieczności wprowadzania założonego rozkładu temperatury ścian pieca i równocześnie stabilizuje obliczenia numeryczne. Wyniki symulacji porównano z dostępnymi wynikami pomiarów przemysłowych.

1. Introduction

In the high temperature pyrometallurgical processes the contribution of radiation mechanism of heat transfer in total transportation of energy can exceed 90%. Exact and inexpensive prediction of energy transfer by radiation is one of the challenging task for the research and development in metallurgical technology. Leading motif of the paper is the simulation of radiation energy transfer in the metallurgical furnaces with emitting-absorbing and scattering media and also explanation of typical phenomena occurring in the furnaces. There are numerous examples of metallurgical processes, when the technological process involves single or multiphase reacting flow at high temperatures. In this paper flash smelting of sulfide copper ores process will be an explanatory example. In flash smelting technology the fine-grained dry copper concentrate oxygenation in co-current flow with furnace blast is the essence of smelting process. The concentrate burner system distributes solid parti-

* DEPARTMENT OF PROCESS ENGINEERING. FACULTY OF NON-FERROUS METALS, AGH UNIVERSITY OF SCIENCE AND TECHNOLOGY, 30 MICKIEWICZA AVE., 30-059 CRACOW

cles of the load in the reaction shaft of the furnace, thus forming the suspension of solid concentrate particles in the oxygen rich blow. An additional oil burner acts as candle to initiate and claim the ignition of particles. Nevertheless, most of the particles are subjected to self-ignition in effect to high thermal radiation exchange. The particles entering the reaction shaft at low temperature (far below ignition temperature) are intensively heated to reach the desired ignition temperature. This is possible by the radiation heat transfer only, because the particles are embedded in the blow gases, fed at low temperature. Then, after ignition, burning particles fall down the reaction shaft, until they are settled on the surface of the furnace bath or on the furnace walls. During their short life in the reaction shaft (2 to 4 sec) they are subjected to chemical conversion (oxidation of combustible species, decomposition of limestone and hydrated compunds, also evaporation of hydrocarbons and moisture water), heat transfer with ambient gases by diffusion and convection, and heat transfer by radiation. Since oxidation reactions are exothermic, the particles acquire high temperature. The excess of particles energy is emitted into the enclosure. The radiation heat transfer can occur between particles, between particle and surrounding emitting-absorbing gases, and between particle and furnace walls or slag surface. This complex scheme of radiation heat transfer is additionally complicated by the accompanying convection and conductive heat transfer.

The presented methods of radiation heat transfer modeling can be applied to many processes involving combustion of solid/liquid particles in the furnace interior.

2. Modeling of multiphase reacting flow

The flow of particles and droplets in fluids occurs very often in industrial processes. The typical high temperature multiphase flow applications are energy conversion and metallurgical processes. For many years, the design of system with particle flows was based primarily on empirical investigations. Increased computational capability has enabled the development of numerical models that can be used to complement engineering system design. The numerical models of multiphase reacting flows are usually based on fundamental principles of momentum, mass and heat transfer. For explanatory purposes, mathematical model of flash smelting process has been documented in details in [1]. A short summary of the model is presented below. The flow of the particles and furnace gases are modeled separately, both are strongly coupled by the momentum, heat and mass transfer phenomena between coexisting phases. The important element of mentioned model is the sub-model of heat transfer in the internal volume of the furnace. It assumes, that the heat transfer in gaseous phase can be described by the classical differential energy equation considering all heat transfer mechanisms (convection, diffusion, radiation). The gaseous phase, the products of combustion and the chemical decomposition (water vapor, carbon dioxide and sulphur dioxide), can absorb and emit energy. The solid/liquid particle phase energy balance also includes all possible modes of energy transfer. These two energy balances are interconnected by heat transfer between phases and boundary conditions. In this paper the radiation transfer problem is considered for the continuous medium composed of a dispersion of particles in the furnace gases. This medium is characterized by the set of common radiant properties, usually calculated using additivity assumption. Then, after the radiant heat transfer model is solved, the resulting heat fluxes are distributed between solid/liquid and gaseous phase using redistribution criteria, based on the same rule. In the absence of solid/liquid dispersed phase the presented numerical techniques can be also applied directly for radiation heat transfer, without additional redistribution of energy fluxes between phases constituting furnace atmosphere.

3. The governing equation of radiative energy transfer with participating media

Thermal radiation as one of the most difficult aspects of the energy transfer problem is usually uncoupled from the other modes of energy transfer to make the heat transfer computations easier. Let us consider the energy equation in combined mode heat transfer process with a participating medium for steady state conditions

$$\nabla \mathbf{q}(\mathbf{x}) + \dot{q}_v(\mathbf{x}) = 0 \tag{1}$$

where $\mathbf{x}$ is a vector of spatial coordinates, $\dot{q}_v(\mathbf{x})$ – space distribution of heat sources, $\nabla \mathbf{q}(\mathbf{x})$ – the divergence of heat flux, which can be expressed in a form revealing three modes of energy transfer (diffusion -*diff*, convection – *conv* and radiation-*rad*):

$$\nabla \mathbf{q}(\mathbf{x}) = \nabla \left((\mathbf{q}_{diff}(\mathbf{x}) + \mathbf{q}_{conv}(\mathbf{x}) + \mathbf{q}_{rad}(\mathbf{x}) \right) = \nabla(-k\nabla T) + \nabla(\rho h \mathbf{v}) + \nabla \mathbf{q}_{rad}(\mathbf{x}) \tag{2}$$

where **v** – velocity vector of flowing media, h – specific enthalpy of media, k – heat conduction coefficient, ρ – density, T – temperature.

The terms representing diffusion and convection depends on local parameters, but the term representing energy transfer by radiation is dependent on local and global distribution of variables defining heat transfer. Simply speaking, the intensity of radiant heat transfer depends not only on local parameters but mainly on spatial distribution of parameters influencing radiation heat transfer in the enclosure. This leads to integro-differential form of energy transport equation, the most difficult equation to be solved. Moreover, the complexity of the radiation transport arises from the fact that the atmosphere of the furnace participates in the radiation transport proportionally to its local properties and global radiation field, and emission, absorption and scattering phenomena must be accounted for. In general, the radiation of matter depends on the wavelength interval as well as on the direction of emission or incidence. In engineering applications, the great simplification of radiation mathematical description is achieved introducing the concept of gray body/substance and the concept of diffusive nature of reflection/emission. The gray surface/substance follows the scaled down Planck blackbody radiation distribution function [2], that simply imply that its directional spectral emissivity is independent on radiation wavelength. The surface/substance is said to be diffuse at a given wavelength, if its directional, spectral emissivity is independent on the direction, and such an assumption is valid along this paper. Thus, the radiant intensity $I(\mathbf{r},\mathbf{s})$ obeys the transport equation for steady-state conditions in the form [2]:

$$\frac{\mathrm{d}I(\mathbf{r},\mathbf{s})}{\mathrm{ds}} = -\kappa(\mathbf{r})I(\mathbf{r},\mathbf{s}) + \sigma_{\mathrm{a}}\mathbf{r}I_{\mathrm{b}}(\mathbf{r},\mathbf{s}) + \frac{\sigma_{\mathrm{S}}(\mathbf{r})}{4\pi}\int_{4\pi} I(\mathbf{r},\varpi_{\mathrm{inc}})\Phi(\varpi,\varpi_{\mathrm{inc}})\mathrm{d}\varpi_{\mathrm{inc}} \tag{3}$$

The left hand side of Eq.(3) represents the spatial changes of the radiant intensity $I(\mathbf{r},\mathbf{s})$ at point **r** in the direction of vector **s** inside solid angle ϖ around vector **s**. The three terms on the right side describe the :

- attenuation of the radiant intensity $I(\mathbf{r},\mathbf{s})$ due to out scattering and adsorption:

$$-\kappa(\mathbf{r})i(\mathbf{r},\mathbf{s})$$

- augmentation of the radiant intensity $I(\mathbf{r},\mathbf{s})$ due to spontaneous emission:

$$\sigma_{\mathrm{a}}(\mathbf{r})I_{\mathrm{b}}(\mathbf{r},\mathbf{s})$$

- augmentation of radiant intensity $I(\mathbf{r},\mathbf{s})$ due to in scattering:

$$\frac{\sigma_{\mathrm{S}}(\mathbf{r})}{4\pi}\int_{4\pi} I(\mathbf{r},\varpi_{\mathrm{inc}})\varphi(\varpi,\varpi_{\mathrm{inc}})\mathrm{d}\varpi_{\mathrm{inc}}$$

where: κ is an extinction coefficient of media, σ_{a} is an absorption coefficient of media, σ_{s} is a scattering coefficient of media, ϖ_{inc} is an angle of incident radiation. The radiation problem in an enclosure can be only solved, when the spontaneous radiation intensities $I_b(\mathbf{r})$ of all enclosing walls are uniquely defined by wall emissivity $\varepsilon(\mathbf{r})$ and its temperature T $(\mathbf{r})$.

When the participating medium contains solid/liquid particles the radiative intensity may be changed by absorption and scattering. Three physical phenomena make contribution to scattering: diffraction, reflection and refraction. How intensive is a single particle scattering depends on the shape of particle, the material of the particle, the relative size of the particle with respect to the radiation wavelength, and the distance from other scattering particles, [2]. For the sake of simplicity, this is common to limit an analysis to spherical particles. The relative size of the particle, described by the size parameter $\delta = \pi d_{\mathrm{p}}/\lambda$ is of great importance in calculation of its radiative properties. For the high temperature pyrometallurgical processes the expected radiation wavelengths mostly contributing to thermal energy transfer lie in the interval of 0.5 to 10 μm. This compared with typical size of particles (pulverized coal, metallurgical dust, concentrate particles in flash smelting process) gives the estimation of δ greater than 5. In this range of δ the Mie scattering theory should be used to evaluate efficiency of scattering, but this would be difficult task due to lack of exact optical properties of particles and cumbersome calculations, [4].

For the gray particles with the value of $\delta > 5$ approximate relationships are suggested, [3]. Usually we have to deal with large collection of particles, forming a suspension. When the average distance between particles is sufficiently greater then radiation wavelength, the scattering by one particle is not affected by the presence of surrounding particles. This condition is usually satisfied in typical metallurgical processes, and the effect of neighbor particles on scattering can be neglected. Thus for the cloud of gray, diffusive and spherical particles of the same diameter d_j, the absorption ($\sigma_{\mathrm{a,j}}$) and scattering ($\sigma_{\mathrm{sc,j}}$) coefficients of the particle cloud can be approximated by

$$\sigma_{a,j} = \frac{\pi}{4}\varepsilon d_j^2 n_j \tag{4}$$

$$\sigma_{sc,j} = \frac{\pi}{4}\rho d_j^2 n_j \tag{5}$$

where: ε, *rho* – gray body emissivity and reflectivity coefficients respectively, n_j – number of particles of uniform diameter d_j in the unit volume of suspension. Since the scattering phase function in a cloud of uniform particles is the same for each particle, it is also the same for the particle cloud.

For clouds of particles of non-uniform size, is customary to approximate absorption and scattering coefficients as a sum of individual particles contribution. So, if the cloud consist of N_f size fractions of particles (uniform diameter d_j), with individual particle density n_j, the summation over all fractions yields

$$\sigma_{a,p} = \frac{\pi}{4}\varepsilon \sum_{j=1}^{Nj} d_j^2 n_j \tag{6}$$

$$\sigma_{sc,p} = \frac{\pi}{4}\rho \sum_{j=1}^{Nj} d_j^2 n_j \tag{7}$$

The extinction coefficient of the cloud p is then expressed by

$$\kappa_p = \sigma_{a,p} + \sigma_{sc,p} \tag{8}$$

The scattering phase function $\Phi(\varpi, \varpi_{inc})$ describe how radiant energy is scattered by a participating medium. Scattering can be classified into two categories: isotropic and anisotropic. Isotropic scattering scatters energy equally into all directions. Anisotropic scattering can be further divided into backward and forward scattering. Backward scattering scatters more energy into the backward direction, while forward scattering scatters more energy into the forward directions. Scattering function must satisfy the following relation:

$$\int_{4\pi} \Phi(\varpi, \varpi_{inc}) d\varpi_{inc} = 4\pi$$

Classical phase function capable to represent all scattering modes can be expressed as a function of an angle between incident and scattered radiation in the form, [4]:

$$\Phi(\varphi) = 1 + a\cos(\varphi) \tag{9}$$

where parameter a can be chosen from the interval [-1,1], Fig.1. When a=0 function (9) describes isotropic scattering, anisotropic backward scattering when a<0, anisotropic forward scattering when a>0. For the spherical, opaque and diffusive scattering solid particles other form of scattering phase function is recommended, [3]:

$$\Phi\varphi = (8/3\pi)(\sin(\varphi) - \varphi\cos(\varphi)) \tag{10}$$

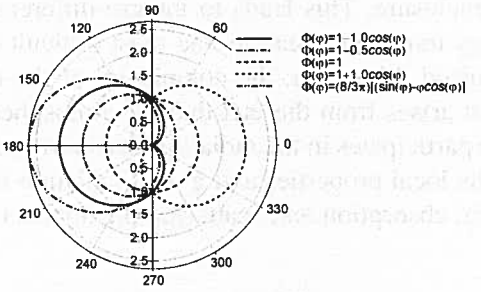

Fig. 1. Scattering phase function in polar coordinates

For non-uniform particles the scattering phase function is not the same for all particles. It was observed, that for the clouds of varying size particles, the phase function becomes very smooth with a strong peek of forward scattering remaining,[2]. Therefore, for whole interval of particle diameter distribution, it is reasonable to use uniform smooth phase function.

The following useful in radiation energy transfer quantities can also be defined [5]:

- the incident radiation G(**r**) at point **r**, where ϖ_{inc} is a solid angle around direction **s**

$$G(\mathbf{r}) = \int_{4\pi} I(\mathbf{r}, \varpi_{inc}) d\varpi_{inc} \tag{11}$$

- the radiant heat flux $E_{rad,i}$ in direction **i**, where ϖ_{inc} is a solid angle around direction **s** of incident radiation

$$E_{rad,i}(\mathbf{r}) = \int_{2\pi} I(\mathbf{r}, \varpi_{inc})(\mathrm{si}) d\varpi_{inc} \tag{12}$$

The divergence of the radiant energy flux, is then related to the intensity of the radiation $I(\mathbf{r},\mathbf{s})$ at the point given by the position-vector **r** by the formula

$$\mathrm{div}\,(\mathbf{q}_{rad}(\mathbf{r})) = \sigma_a(\mathbf{r})[4\pi I_b(\mathbf{r}) - G(\mathbf{r})] = 4\pi\sigma_a(\mathbf{r})I_b(\mathbf{r}) - \sigma_a(\mathbf{r}) \int_{4\pi} I(\mathbf{r}, \varpi_{inc}) d\varpi_{inc} \tag{13}$$

where the integral term expresses the adsorption of the incident radiation from all directions.

The solution of the radiant heat transfer requires adequate boundary conditions. The radiant intensity leaving an opaque diffuse surface contains emitted and reflected energy, what can be expressed by

$$I(\mathbf{r},\mathbf{s}) = \varepsilon(\mathbf{r})I_b(\mathbf{r}) + \frac{\rho(r)}{\pi}\int_{\mathbf{n}\cdot\mathbf{s}'<0} I(\mathbf{r},\varpi_{inc}) \mid \mathbf{n}\mathbf{s}' \mid d\varpi_{inc} \tag{14}$$

where ε – wall emissivity, ρ – wall reflectivity, **s'** – direction of incident radiation, ϖ_{inc} – the solid angle around direction **s'**, **n** – normal to wall vector, $\mathbf{s}\,\mathbf{n} < 0$ – denotes summation over all direction **s'** in the hemisphere convex into direction of **n**.

4. Numerical solution of radiant energy transport

A very important aspect of the modeling of high temperature processes is to solve the radiation transfer problem accurately and efficiently, because of the dominant role of this mode of energy transfer. Any of the numerous solution techniques for the emitting, absorbing and scattering media can be exploited. Hottel's zone method [6] is the classic one, provides a complete solution for the gray media, but is computationally intensive and expensive. The Monte Carlo ray tracing method [4] offers great versatility and accuracy, at a price of expensive computations. The flux method, the finite volume and the discrete ordinates method has gained popularity due to relative simplicity and its consistency with space discretization used for the numerical solution of transport equations. The concept of finite volume method and discrete ordinates method for radiation heat transfer is based on the similarity of radiant heat transfer equation and the following form of general transport equation for dependent variable ψ(x,y,z) (steady state assumed for simplicity):

$$\rho u\frac{\partial\psi}{\partial x} + \rho v\frac{\partial\psi}{\partial y} + \rho w\frac{\partial\psi}{\partial z} = \frac{\partial}{\partial x}\left(\Gamma\frac{\partial\psi}{\partial x}\right) + \frac{\partial}{\partial y}\left(\Gamma\frac{\partial\psi}{\partial y}\right) + \frac{\partial}{\partial z}\left(\Gamma\frac{\partial\psi}{\partial z}\right) + (S_1 + S_2\psi) \tag{15}$$

Transport of mass, momentum and energy is usually described by the partial differential equations which can be considered as special cases of general transport equation. In the absence of diffusion ($\Gamma = 0$) and for constant values of $\rho u = c_x$, $\rho v = c_y$, $\rho = c_z$ the Eq. (15) takes the form:

$$c_x\frac{\partial\psi}{\partial x} + c_y\frac{\partial\psi}{\partial y} + c_z\frac{\partial\psi}{\partial z} = (S_1 + S_2\psi) \tag{16}$$

The radiation transport equation (3) written for a rectangular three-dimensional enclosure containing a gray, absorbing, emitting, and scattering medium takes similar form:

$$l\frac{\partial I(\mathbf{r},\varpi)}{\partial x} + m\frac{\partial I(\mathbf{r},\varpi)}{\partial y} + k\frac{\partial I(\mathbf{r},\varpi)}{\partial z} = -\kappa(\mathbf{r})I(\mathbf{r},\varpi) \tag{17}$$

if the source term S_3 consists of a sum of spontaneous irradiation and scattering terms

$$S_3(\mathbf{r},\varpi) = \sigma_a(\mathbf{r})I_b(\mathbf{r}) + \frac{\sigma_S(\mathbf{r})}{4\pi}\int_{4\pi} I(\mathbf{r},\varpi_{inc})\Psi(\varpi,\varpi_{inc})d\varpi_{inc} \tag{18}$$

The constants l=cosα, m=cosβ, k=cosγ appearing in (17) are the direction cosines of vector **s**, where α, β, *gamma* are angle values between vector **s** and axis unit vectors of coordinate system.

The similarity between general transport equation and radiation transport equation (16) is obvious. It makes possible standardization of numerical solution techniques for all transport equations in the computer flow dynamics (CFD) software.

Since the radiant intensity $I(\mathbf{r},\mathbf{s})$ is a continuous function of direction angle and spatial coordinates, numerical solution of radiant energy transport equation (3) requires discretization in both the angular and spatial domains. The numerical methods for solving radiation transport equation differ in the angular discretization schemes. The flux method, first proposed for 1-dimensional radiative transfer, then extended by Chu and Churchill [7] for 3-dimensional problems, assumes that the radiation is allowed to travel in all directions within each solid angle. When several control angles are introduced in each coordinate directions, the flux method switches to control volume method. Better approximation to radiation transfer in the case of anisotropic scattering problems can be attained by the discrete ordinate method, where the actual radiation field is divided into a finite number of discrete directions. For schematic comparison of discretization of radiant intensity distribution among mentioned numerical methods see Fig.2.

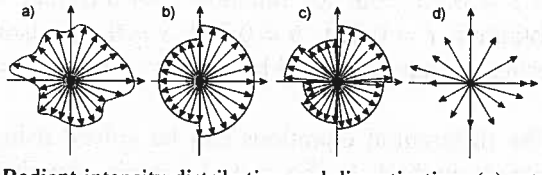

Fig. 2. Radiant intensity distribution and discretization: (a) actual intensity distribution, (b) flux method discretization, (c) finite volume discretization, (d) discrete ordinate method discretization

The flux method

Let us assume that for simplicity the scattering in 2-dimensions is approximated by the formula

$$\int_{4\pi} I(\mathbf{r}, \varpi_{\text{inc}})\Psi(\varpi, \varpi_{\text{inc}})\mathrm{d}\varpi_{\text{inc}} = 4\pi(I_+(\mathrm{r})f + I_-(\mathrm{R})b) \tag{19}$$

where f and b are the fractions of energy scattered in forward and backward directions, $I_+(\mathbf{r})$ and $I_-(\mathbf{r})$ are intensities traveling in positive and negative directions respectively. When isotropic scattering occurs $f = b = 1/2$.

Integration of radiant transport equation (3) over the positive and negative coordinate hemisphere (solid angle 2π) leads to the set of differential equations for unknown radiative heat fluxes E (defined by (12))[6,9]:

$$\frac{1}{2}\frac{dE_+(\mathbf{r})}{\mathrm{dx}} = -\kappa(\mathbf{r})E_+(\mathbf{r}) + \frac{1}{2}a(\mathbf{r})E_b(\mathbf{rf}) + \sigma_S(fE_+(\mathbf{r}) + bE_-(\mathbf{r})) - \frac{1}{2}\frac{dE_-(\mathbf{r})}{\mathrm{dx}} = -$$

$$= -\kappa(\mathbf{r})E_-(\mathbf{r}) + \frac{1}{2}a(\mathbf{r})E_b(\mathbf{rf}) + \sigma_S(fE_+(\mathbf{r}) + bE_-(\mathbf{r})) \tag{20}$$

where E_b – black body emission from isothermal unit volume of media, ($E_b = 4\pi I_b$), E_+ – radiative flux in positive coordinate direction, E_- – radiative flux in negative coordinate direction.

When the 3-dimensional enclosure is under consideration, similar procedure leads to the following set of differential equations:

$$\begin{aligned}
\tfrac{1}{\kappa}\tfrac{dE_{x+}}{dx} &= -(1-\Omega f)E_{x+} + \Omega bE_{x-} + \Omega s(E_{y+} + E_{y+} + E_{z+} + E_{z+}) + \tfrac{1}{6}(1-\Omega)E_b \\
\tfrac{1}{\kappa}\tfrac{dE_{x-}}{dx} &= -(1-\Omega f)E_{x-} + \Omega bE_{x+} + \Omega s(E_{y+} + E_{y+} + E_{z+} + E_{z+}) + \tfrac{1}{6}(1-\Omega)E_b \\
\tfrac{1}{\kappa}\tfrac{dE_{y+}}{dy} &= -(1-\Omega f)E_{y+} + \Omega bE_{y-} + \Omega s(E_{x+} + E_{x+} + E_{z+} + E_{z+}) + \tfrac{1}{6}(1-\Omega)E_b \\
\tfrac{1}{\kappa}\tfrac{dE_{y-}}{dy} &= -(1-\Omega f)E_{y-+} + \Omega bE_{y+} + \Omega s(E_{x+} + E_{x+} + E_{z+} + E_{z+}) + \tfrac{1}{6}(1-\Omega)E_b \\
\tfrac{1}{\kappa}\tfrac{dE_{z+}}{dz} &= -(1-\Omega f)E_{z+} + \Omega bE_{z-} + \Omega s(E_{z+} + E_{z+} + E_{y+} + E_{y+}) + \tfrac{1}{6}(1-\Omega)E_b \\
\tfrac{1}{\kappa}\tfrac{dE_{z-}}{dz} &= -(1-\Omega f)E_{z-} + \Omega bE_{z+} + \Omega s(E_{x+} + E_{x+} + E_{y+} + E_{y+}) + \tfrac{1}{6}(1-\Omega)E_b
\end{aligned} \tag{21}$$

where: E_{x+}, E_{x-}, E_{y+}, E_{y-}, E_{z+}, E_{z-}, are radiative heat fluxes in both directions of Cartesian coordinate system, $\Omega = \sigma_s/(\sigma_a + \sigma_s)$ – is an albedo factor of the medium, $\kappa = \sigma_a + \sigma_s$ – is a total absorption and out-scattering coefficient of the medium (extinction coefficient). The dependence of all variables in (21) on position vector $\mathbf{r}$ has been omitted for the notation purpose. The f, b, s factors of 6-flux method [7], describing scattered fractions of radiant energy in all direction (forward, backward, sideward), can be easily obtained by integration of scattering phase function $\Psi(\varpi, \varpi_{\text{inc}})$ over incident radiation angle ϖ_{inc}. For example, when scattering function is defined by (9) with $a = 1$ (dominant backscatter) , 6-flux approximation coefficients attain values: $f = 0.042$, $b = 0.292$, $s = 0.167$, but for function (10) different values are obtained: $f = 0.021$, $b = 0.354$, $s = 0.156$. Isotropic scattering is then described by the set: $f = 1/6$, $b = 1/6$, $s = 1/6$.

The differential equations can be solved using any convenient method. In the spatial domain equations are discretized into finite number of control volumes. Discretization of Eq.(21) must be applied for each control volume, thus delivering the set of difference equations, and after that any of algebraic equation solver can be used. But, to simplify the solution procedure, the following reconstruction of the problem has been proposed [8]. An introduction of net radiative energy fluxes along coordinate system axes:

$$Q_x = E_{x+} - E_{x-}, Q_y = E_{y+} - E_{y-}, Q_z = E_{z+} - E_{z-} \tag{22}$$

and summing up in pairs Eqn's (21), one can obtain the reduced system:

$$\begin{aligned}
\tfrac{1}{\kappa}(dQ_x/dx) &= CF_x + W(F_y + F_z) + HE_b \\
\tfrac{1}{\kappa}(dQ_y/dy) &= CF_y + W(F_x + F_z) + HE_b \\
\tfrac{1}{\kappa}(dQ_z/dz) &= CF_z + W(F_z + F_y) + HE_b
\end{aligned} \tag{23}$$

where: $C = -(1 - \varpi f - \varpi b)$; $D = (1 - \varpi f + \varpi b)$; $W = 2\varpi s$; $H = \frac{2}{6}(1 - \varpi)$. Introducing radiative energy fluxes defined by:

$$F_x = E_{x+} + E_{x-}, F_y = E_{y+} + E_{y-}, F_z = E_{z+} + E_{z-} \tag{24}$$

and now subtracting in pairs Eqn's (21) yields:

$$\frac{1}{\kappa}(dF_x/dx) = -DQ_x, \frac{1}{\kappa}(dF_y/dy) = -DQ_y, \frac{1}{\kappa}(dF_z/dz) = -DQ_z \tag{25}$$

Combining Eqn's (23) and (25), leads to the set of second order differential equations set:

$$
\begin{aligned}
-\frac{d}{dx}\left(\frac{1}{D\kappa}\frac{d}{dx}(F_x)\right) &= CF_x + W(F_y + F_z) + HE_B \\
-\frac{d}{dy}\left(\frac{1}{D\kappa}\frac{d}{dy}(F_y)\right) &= CF_y + W(F_z + F_z) + HE_B \quad (26) \\
-\frac{d}{dz}\left(\frac{1}{D\kappa}\frac{d}{dz}(F_z)\right) &= CF_z + W(F_y + F_z) + HE_B
\end{aligned}
$$

with unknown spatial distribution of radiative energy fluxes F_x, F_y, F_z .

The boundary conditions for Eqn's (26) can be derived from radiant energy balance at the solid surface (14) in the form (only x_+ direction is displayed as an example):

$$E_{x+} = \varepsilon_s e_b(T) + \rho_s E_{x-} = \varepsilon_s e_b(T) + (1 - \varepsilon_x)E_{x-} \quad (27)$$

where: ε_s – emissivity of the gray surface, ρ_s – reflectivity of the gray surface, (transmissivity has been assumed to be zero), e_b – hemispherical total emission of the black surface at absolute temperature T. Introduction of new variables (22) and (24) into (27) gives the form of boundary condition, to be used in connection with (26):

$$\frac{1}{2}(F_x + Q_x) = \varepsilon_s e_b + (1 - \varepsilon_s)\frac{1}{2}(F_x - Q_x) \quad (28)$$

The additional boundary conditions can be imposed on the symmetry plane of the problem under consideration:

$$\frac{dF_n}{dn} = 0 \quad (29)$$

where: n is equal to x or y or z, depending of the position of symmetry plane.

The discrete formulation of the problem, i.e. Eqn's (26), together with boundary conditions of type (28) and (29), is a typical boundary value problem of the second order differential equations. It can be solved easily using any of the numerical method, once the temperature and radiation properties distributions of participating media are known in the system under consideration. For the central difference scheme on rectangular grid it forms the 3-three-diagonal system of algebraic equations, coupled by the source terms (right and sides of the Eqn's (26)). Therefore, iterative solution technique is recommended, starting from guessed distribution of unknown fluxes F, or, when the radiation transport problem is a part of overall energy conservation problem, the restart of radiation transport calculations can be initialized from the previously obtained distribution of F and T.

The final objective of the radiation energy transfer problem is the evaluation of the radiant energy flux divergence distribution in space. The solution of the boundary value problem (26) and (28) and (29) can be directly utilized for this purpose, since

$$div(\mathbf{q}_{rad}) = -\sigma_a(F_x + F_y + F_z - 4\pi I_B \quad (30)$$

according to (13) and approximation used:

$$\sigma_a \int_{4\pi} \mathrm{I}(\mathrm{r}, \varpi_{\mathrm{inc}})\mathrm{d}\varpi_{\mathrm{inc}} = \sigma_a(F_x + F_y + F_z) \quad (31)$$

The discrete ordinates method

The flux method could not accurately model anisotropic scattering with its solid angle discretization practice. The discrete ordinates method, originated from the same idea, offers greater flexibility in fitting appropriate discretization to the resolved problem, to achieve required accuracy. In the discrete ordinates approximation the integrals appearing in the source term S_3, Eq. (18) , are approximated as weighted sums of the set of M incident discrete intensities

$$\int_{4\pi} I(x, y, z, \varpi_{inc})\Psi(\varpi, \varpi_{inc})d\varpi_{inc} = \sum_{m_{inc}=1}^{M} A_{m_{inc}} I_{m_{inc}} \Psi_{m,m_{inc}} \quad (32)$$

scattered in the direction of ϖ(intensity I_m). An index m_{inc} is associated with incident direction of radiation (ϖ_{inc}).

Using appropriate numerical integration scheme, namely Gauss formula [9] or other proposed in [5,10,11], one can obtain weighting factors A_{m} associated with the direction m_{inc}. Number of chosen directions M dictates the number of differential radiation transport equation to be solved simultaneously to obtain closed system of equations uniquely defining the set of discrete intensities I_{m}. Thus, equation (3) is approximated by a set of M equations:

$$
\begin{aligned}
\mathbf{I_m}\frac{\partial I_m(x,y,z)}{\partial x} + \mathbf{m_m}\frac{\partial I_m(x,y,z)}{\partial y} + \mathbf{n_m}\frac{\partial I_m(x,y,z)}{\partial z} &= \quad (33) \\
-\kappa I_m(x, y, z) + \sigma_a I_b(T) + \frac{\rho_w}{\pi}\sum_{\mathbf{ns}j} A_j I_j(x_w, y_w, z_w) \mid \mathbf{ns}_j \mid & \quad (33)
\end{aligned}
$$

where: m=1,2,...,M, and $\mathbf{I}_m$, $\mathbf{m}_m$, $\mathbf{n}_m$ – m direction cosines in rectangular coordinates. Boundary conditions in the form of Eq. (14) can be analogously discretized in a solid angle space to close radiation transport problem:

$$I_m(x_w, y_w < z_w) = \varepsilon_w I_b(T_w) + \frac{\rho_w}{\pi}\sum_{\mathbf{ns}_j} A_j I_j(x_w, y_w, z_w 0 \mid \mathbf{ns}_j \mid \quad (34)$$

where: m – the direction index for the radiation beam emanating from the wall (i.e. $\mathbf{n}\ \mathbf{s}_j > 0$), while summation is carried out over radiation beams striking the wall (i.e. $\mathbf{n}\ \mathbf{s}_j < 0$).

This is interesting to note, that as Eq. (33) form the set of first order differential equations. It requires only one boundary condition per unknown intensity I_m. The

boundary conditions (34) are defined for the intensities emanating from the wall, what is sufficient condition to make the solution of the problem unique.

If the scattering of the medium is present, the equations are coupled through the scattering term and should be solved using iterative procedure. The same situation takes place, when the temperature distribution is unknown.

The choice of numerical integration scheme (32) of scattering energy term is arbitrary. But, the observed uncertainty of some numerical quadratures, imposes additional restrictions on directions and quadrature weights. Interested reader is directed to study some research papers on this topic , i.e. [2,10,11]. One general rule has to be fulfilled. As a reminiscence of two flux method, each radiation beam passing in one direction (ordinate) must be accompanied by the second passing in the opposite direction. Therefore, the ordinates appear in pairs and so M must be an even number. It become customary to designate the quadrature approximation degree by S_n, where the number of ordinates $M = n(n + 2)$. For S_4 approximation 24 ordinates are in use (3 per octant of the sphere), but for S_6 number of ordinates amounts to 48 (6 per octant). Then, each equation for the intensity in direction m, is discretized in usual manner on the finite difference grid to obtain algebraic equation set for the distribution of discrete intensity I_m over the grid nodes. For the rectangular grid, integration of Eq. (17) over the volume of grid element $\Delta x\Delta y\Delta z$, yields the following difference equation for the distribution of intensity I_m:

$$\begin{aligned}\mathbf{I}_m\Delta y\Delta z(I^P_{m,x+} - I^P_{m,x-}) + \mathbf{m}_m\Delta x\Delta z(I^P_{m,y+} - I^P_{m,y-}) + \mathbf{n}_\mathbf{m}\Delta Y\Delta x(I^P_{m,z+} - I^P_{m,z-}) = \\ -\kappa^P\Delta x\Delta y\Delta z I^P_m + \sigma^P_a\Delta x\Delta y\Delta z I_b(T^P) + \tfrac{\sigma^P_s}{4\pi}\Delta x\Delta y\Delta z\sum_{m\prime=1}^{M} A_m, I^P_{m\prime}, \Psi_{m\prime,m}\end{aligned} \tag{35}$$

where: m=1,2,... M, $I^P_{m,x+}$, $I^P_{m,x-}$, $I^P_{m,y+}$, $I^P_{m,y-}$, $I^P_{m,z+}$, $I^P_{m,z-}$ – intensity I_m values at the control element surfaces, I^P_M – nodal value of I_m at central point of the control element. The surface values of radiant intensities at the control element surfaces can be evaluated on the linearity assumption of the inter-element intensity distribution

$$I^P_m = \frac{1}{2}\left(I^P_{m,x+} + I^P_{m,x-}\right) = \frac{1}{2}\left(I^P_{m,y+}I^P_{m,y-}\right) = \frac{1}{2}\left(I^P_{m,z+} + I^P_{m,z-}\right) \tag{36}$$

In general, the equations are strongly coupled, and the boundary conditions contain the unknown intensity values, therefore it is necessary to solve the system iteratively, starting from guessed intensity distribution. The equations (35) and (34) can be solved easily using explicit evaluation of I^P_m, if solved in correct sequence (i.e. starting from alternating corners of the domain, always marching in downstream beam direction). During iterative solution some predicted finite element face intensities could become negative. This is due to extrapolation using Eq. (36). Setting negative values to zero, and continuing computation is generally accepted, but this may lead to oscillations and instability. The negative values can be avoided imposing upper bound on finite volume dimensions Δx, Δy, Δz as proposed in [13]. After the distribution of al grid nodal intensities I_m are known, the procedure is repeated, until convergence criteria are satisfied.

Approximation errors

The outlined methods can be used to solve steady-state radiation transfer problems that can be described in Cartesian coordinates. Irregular geometries can be handled using staircase-like boundary approximation or spatial-multi-block division of the domain. This class of the numerical solution procedures can be effectively used in many practical problems, however, similar to other numerical methods, they are exposed to discretization errors. The numerical discretization of angular space is inherently biased by the ray effect [5]. The ray effect arises from approximating the continuously varying angular nature of radiation with a discrete set of angular directions, and is independent of spatial differencing scheme. The spatial differencing practice can produce false numerical scattering. In computer fluid dynamics this phenomenon, called numerical diffusion, is often encountered. Numerical scattering results in deformation of predicted intensity profile and in excessive smoothing of radiation field. It can be reduced by applying finer spatial grid. This must be accompanied by the finer discretization of angular space (more discrete ordinates) to avoid errors produced by the ray effect [5].

Integration with combined mode heat transfer

Outer iterations are needed for the solution of coupled diffusion, convection and radiation heat transfer problem for any of the numerical method used for radiation transfer problem. Thus, the single outer iteration step composes of the solution of energy balance equation (1) and the solution of radiation transfer equation (3). The equations are two-way coupled through divergence of radiation flux (13) and temperature distribution in space. Special attention should be devoted to the accurate formulation of the boundary condition for energy transfer, as a radiation transfer is highly dependent on temperature distribution. In this study, there was assumed that, the combined heat transfer problem involves the energy transfer to the wall by means of:

radiation, diffusion and convection, and through settling of the solid/liquid particles of different temperature on the wall surface. This combined energy transfer, in conjunction with rectangular structured grid, when curved walls are approximated by staircase-like geometries, can produce locally discontinuous distribution of the wall temperatures, disturbing smooth convergence of iterative solution procedure. Auxiliary heat transfer model (diffusion heat transfer) in the furnace walls should serve as a simple remedy for this problem. When the intensive cooling is imposed on the outer surfaces of the furnace walls (for example water spraying system is used on the external surfaces of the flash smelter reaction shaft), the necessary smoothing of wall temperature distribution is obtained.

5. Simulation results

Both, the 6-flux model and the discrete ordinates model of radiant energy transfer has been implemented in the software package for the simulation of metallurgical processes. The set of procedures for calculation of the distribution of energy sources due to radiation heat transfer in the participating media serves as an independent sub model of the furnace mathematical model. Prior to the final consolidation of radiation heat transfer model with the CFD code, the necessary testing calculations has been performed. Usually, this is made for selected benchmark problems, having known reliable solutions as a reference. The numerical procedures were prepared for 3D calculations. Therefore, when tested cases were defined for simplified geometries (1D or 2D), simulation has been carried out for appropriate 3D enclosure, preserving sufficiently large dimension of analyzed domain in the directions perpendicular to planes in original test cases. As a first test problem (test case No1), let us consider the two infinite, parallel walls, spaced a distance L and maintained at temperatures T_0=900 K and T_L = 300 K. The temperature distribution in absorbing and emitting medium is set to be linear with the distance x from the wall

$$T(x) = 700 - 300(x/L) \quad for \quad x \in (0, L)$$

The discontinuity of temperature distribution at the walls is reasonable only when the heat transfer by conduction or convection is neglected [2], how it was assumed in the test case. The task is to calculate the net radiative flux density distribution in the space between walls, if the medium is assumed to be gray with absorption coefficient κ =0.15 [1/m]. The reference solution has been obtained using 2-flux method for 10 space zones [4]. The comparison of the results are shown in Fig.3.

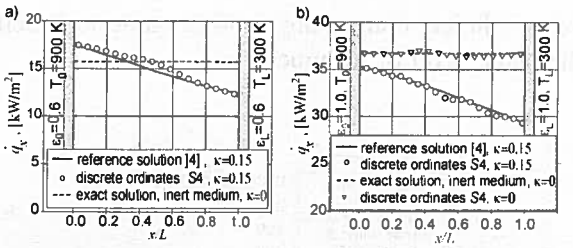

Fig. 3. The net radiative heat flux profiles for: (a) black gray surfaces, (b) black surfaces

In the next test case (No.2), the distribution of heat flux on the surface of the rectangular enclosure is to be calculated. The flat enclosure is build up from ideal black surfaces kept at constant temperature T = 0. Two particular variants are assumed: an absorbing-emitting media at constant temperature T_g=500 K, (case No.2a) and the same media with an unknown temperature (one wall has constant nonzero temperature 500°C, case No.2b). In the second variant temperature can be obtained from the balance of radiant energy based on the hypothesis of radiation equilibrium [2]. Different absorption coefficient has been used in computation and results are shown in Fig.4.

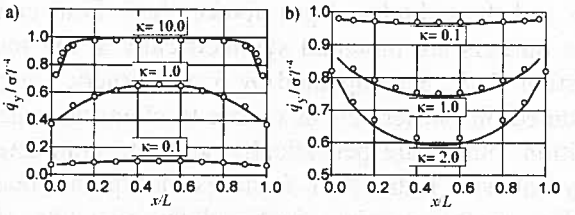

Fig. 4. Distribution of normalized wall heat flux: (a) normalized by medium temperature, (b) normalized by wall temperature (hot wall). Solid lines – numerical solution using discrete ordinates method S4, circles – reference solution [11]

Test case No 3 – the ideal furnace, [12]. The geometry of the furnace is simplified to the rectangular prism (2*times*2×4 m) with gray and diffuse walls. All the walls, except those perpendicular to long furnace axis z, have equal temperatures and emissitivities (T = 900K, ε = 0.7). The wall at z=4 characterizes T=1200 K, ε=0.85, and the wall at z=0 has T=400, ε=0.70. The furnace is filled with absorbing and emitting media (absorption coefficient κ=0.5 m^{-1}). In the furnace interior the uniform heat source distribution is assumed, $\dot{q}_v$ = 5 $kW \cdot m^{-3}$. The distribution of heat fluxes at the mid-height of the hot and cold wall are compared with reference solutions [14,15], Fig.5a. The temperature distribution, calculated using hypothesis of radiation equilibrium is shown in Fig. 5b .

Inspection of presented solutions of test cases authorize us to assume that the prepared sub-model of radiation transfer is a reliable tool for simulation radiation heat transfer with participating media. The calculations

are very efficient comparing to other numerical methods of the same level of accuracy.

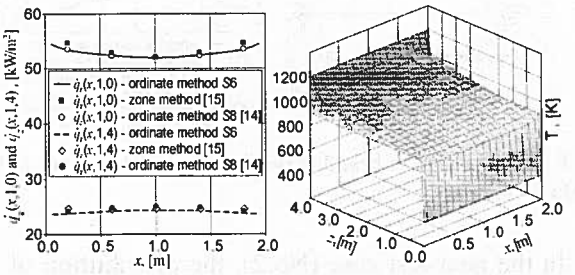

Fig. 5. The solution of test case 3. (a) heat fluxes on the walls, where: solid lines – discrete ordinate solution, circles – reference solutions [14,15], (b) temperature distribution of media (20^3 volume grid, 48 ordinates)

6. Multiphase flow with radiation – flash smelting example

The short description of the flash smelting process has been delivered in the paper introduction. The furnace consist of cylindrical reaction shaft (7m diameter, 7m height), the parallelepiped settler for the smelted products and the cylindrical gas uptake shaft. Four concentrate burners are mounted symmetrically at the roof of reaction shaft, accompanied by 5 oil burners. Centrally mounted oil burner acts as candle to claim the particles ignition, others are periodically active to complete energy balance. Today flash furnaces incorporate massive cooling in the reaction shaft and the slag line of the settler. Cooling elements are also used in the vicinity of burners and trapping runners entrance, even in some fragments of gas uptake shaft. Good knowledge of the distribution of heat generation intensity and heat transfer mechanism, the fluid dynamics of the particle suspension, physical and chemical properties of lining materials is essential in designing the furnace cooling system. The flow of solid/liquid particles through the confined inner furnace space is accompanied by the particles collision with the furnace walls. Depending on local flow and thermal conditions in the vicinity of the wall surface and wall temperature itself, the accretion formation or wall surface corrosion can occur. In the first case, formation of infusible accretions on cold walls restrains the suspension flow and heat removal from the furnace; both phenomena contribute to shortening of the furnace production campaign.

The presented results of simulation of radiation heat transfer in the flash smelter are based on the set of data, delivered by complete model of single-stage flash smelting process [1]. These are spatial distributions of: the particles number density (concentration) for all analyzed size fractions Fig.6, the spatial concentration of gaseous constituents Fig.7, gas temperature Fig.8a, particles temperatures and mass flux of product settled on or crossing the furnace model domain boundaries Fig.9.

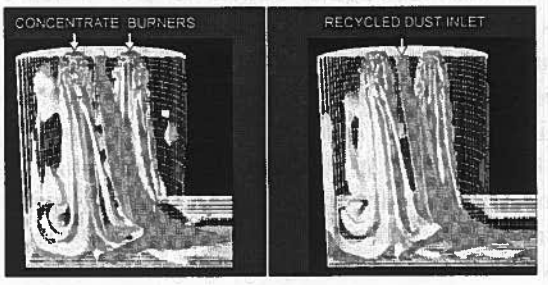

Fig. 6. Particles number concentrations. (a) iso-surface of 3×10^8 [m^{-3}], d=50 μm (b) iso-surface 6×10^9 [m^{-3}], d=20 μm

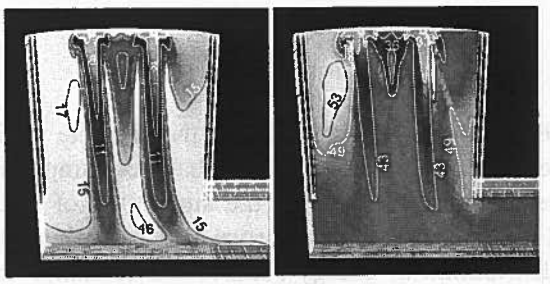

Fig. 7. Gas components concentrations (%wt). (a) SO_2, (b) CO_2

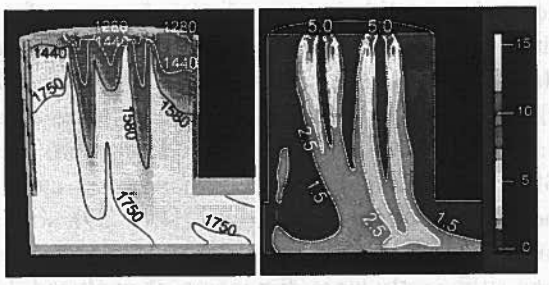

Fig. 8. Temperature distribution [K] (b) Particles cloud absorption coefficient [1/m]

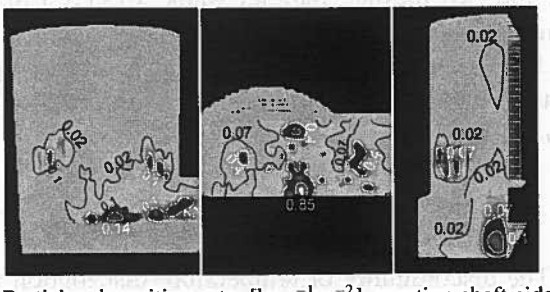

Fig. 9. Particles deposition rate, [kg·s^{-1}m^{-2}], reaction shaft side wall -left, slag surface – center, reaction shaft back wall – right

The radiant properties of particles cloud has been calculated using approximate formulas (6) and (7). The distribution of particle cloud absorption coefficient is presented in Fig.8b. The absorption coefficient of furnace gas can be related to the gas emissivity through the formula

$$\sigma_{a,gas} = -\left(\ln(1-\varepsilon_{gas})\right)/L_{gas}$$

where: emissivity coefficient has been evaluated as a function of partial pressures of active (absorbing/emitting) gas components (SO_2,CO_2,H_2O) using Leckner formula [16], L_{gas} is the mean radiation beam penetration distance based on geometry of the enclosure. The absorption coefficient of gas is less of one order of magnitude in comparison to the absorption coefficient for the particle cloud.

When the energy transfer in the gas phase and solid phase are separately resolved, there is necessary to define the rule of redistribution of radiant energy transfer between two coexistent phases. With the lack of precise knowledge, the simple additive rule can be applied. Thus, if the total absorption coefficient of the suspension is a sum of absorption coefficients of the gas phase and particle phase

$$\sigma_a = \sigma_{a,p} + \sigma_{a,gas}$$

the radiant energy transfer distributes between phases proportionally to the ratios of the phase absorption coefficients related to the total absorption coefficient of the suspension. It means that only the fraction $\sigma_{a,gas}/\sigma_a$ of divergence of total radiation flux (13) must be inserted into energy equation for gas phase as a source term. The rest is used in the energy equation of solid/liquid dispersed phase.

The combustion of oil from auxiliary burners has been modeled using uniform oil droplets dimension and standard Lagrange equation of motion, accompanied by the combustion kinetic model based on hydrocarbons evaporation rate and oxygen diffusion rate to the combustion reaction front [17].

The emission and absorption of radiant heat flux of particles are presented in Fig.10. This is interesting to observe that the particles entering the furnace volume are intensively heated by radiation, then after ignition, give back energy to the enclosure. In the core of concentrate burner flames, where intensity of combustion is restricted by oxygen concentration in furnace gases, the particles are absorbing energy by radiation along their way up to the slag surface.

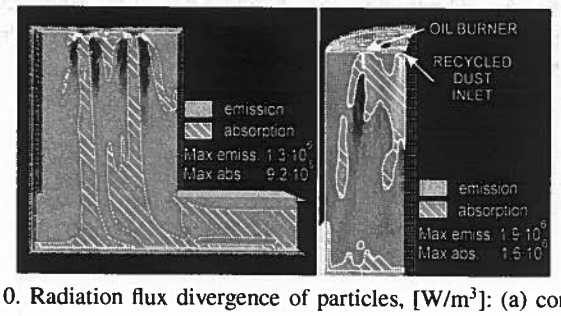

Fig. 10. Radiation flux divergence of particles, [W/m^3]: (a) concentrate burner axis cross-section, (b) oil burner and recycled dust inlet cross-section

The energy transfer equation in the gas phase is coupled with the model describing heat transfer processes inside the furnace walls to attain more reliable wall surface temperature distribution taking also into account leveling of walls temperature induced by furnace cooling system. This extension of the model domain is necessary, when the simulations is to be used for the design of complex cooling system (location of caissons, water sprinkle system). The resulting from calculations wall temperature distribution is shown in Fig.11a., where for comparison, the measured external surface wall temperatures are presented in Fig.11b. The steel shell of the shaft is cooled by the flowing-off water film. The measurements were conducted using special sensors (Kemtherm HFM®) appropriate for these conditions. The distribution of measured isotherms is much alike as the layout of calculated one. The predicted heat flux to surroundings on the reaction shaft furnace in the range of [25÷75 kW·m^{-2}] agree well with industrial measurements data showing the horizontal like contour line distribution in the range of [15÷65 kW·m^{-2}].

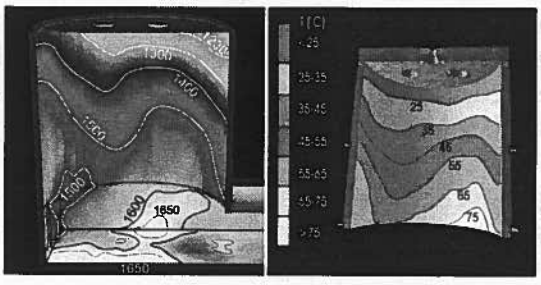

Fig. 11. Temperature distribution on the surface of the reaction shaft walls: (a) predicted on the internal surfaces, [K] (b) measured on the external steel shell surface, [C]

The discrepancies observed in the values of heat flux at the bottom of the shaft are due to the action of caissons mounted in the base of shaft walls. The industrial measurements has been conducted on the external steel shell, thus the measurement results in the vicinity of caissons are less then those predicted on the internal surface. It is interesting to observe, that the maximal predicted temperatures of the internal surfaces of the furnace enclosure are located in regions where the dense hot particles cloud is flowing very close to the wall (back wall of the settler and reaction shaft, base of the reaction shaft) and in the regions where particles are settled (surface of the slag and selected places on the settler and reaction shaft walls). In the energy transfer calculations, the energy balance of the wall includes the excess of energy carried by the particles settled on the wall. Hot particles produce higher temperature of the wall.

The distribution of wall temperature points out areas of furnace wall surfaces, where the accretion formation is probable. The critical condition can be imposed by the temperature of the wall. Formation of high fusible magnetite is thermodynamically favored below 1473 K, [18]. If the particles, already melted in the furnace, are settled on the too (excessively) cold wall the accretion is likely to be formed. These areas are located at the junction of the reaction shaft roof and vertical walls, and exhibits axial asymmetry. This is caused by the unsymmetrical flow of the suspension in the reaction shaft, the large recalculation of hot gases and particles is predicted along the back wall of the smelter.

7. Conclusions

An implementation of flux method and discrete ordinate method of solving radiation heat transfer in the metallurgical full scale industrial process has been presented. The obtained results confirm the applicability of the methods for engineering design purposes. An analysis of chemical and physical processes (combustion, evaporation, etc.), where temperature controls the rate of phenomena, the accurate temperature distribution in radiation participating media is required to obtain reliable predictions. However, full model verification for industrial process (like flash smelting) is often impossible due to limited availability of measurements data. Comparison of predicted temperature and heat loses distribution from the walls remain in reasonable agreement with those resulted from industrial measurements.

The relative high efficiency and easy integration into computer fluid dynamics (CFD) codes is a great advantage of these methods. For the complex furnace geometry and cooling system the application of auxiliary heat transfer model in the furnace walls should be advised. Coupling energy transfer in interior enclosure of the furnace with exterior heat transfer trough energy balance at the internal walls removes dependence of the modeling results on arbitrarily chosen distribution of wall temperatures. In this way more accurate results are obtained and the modeling tasks could be extended to the analysis of cooling system design. Several other profits of advanced process simulation have been discussed using flash smelting process modeling as an example.

Received: 10 February 2008.

Acknowledgements

The financial support of the Ministry of Science and Higher Education under the contract no 11.11.180.375 is gratefully acknowledged.

REFERENCES

[1] J. Donizak, A. Hołda, Z. Kolenda, Progress in Computational Fluid Dynamics **5**, 3/4/5 (2005).
[2] M. F. Modest, Radiative Heat Transfer, Mc Graw-Hill Co. (2000).
[3] H. C. Hottel, A. F. Sarofim, Radiative Transfer, McGraw-Hill Co., NY (1967).
[4] J. Mahan, J. Robert, Radiation Heat Transfer. A Statistical Approach., John Wiley & Sons Inc., NY (2002).
[5] J. C. Chai, S. V. Patankar, Handbook of Numerical Heat Transfer, 2nd Ed., Eds.: W. J. Minkowycz, E. M. Sparrow, J. Y. Murthy, John Wiley & Sons Inc. (2006).
[6] R. Siegel, J. R Howell, Thermal Radiation Heat Transfer, Hemisphere, NY (1981).
[7] Chiao-Min Chu, S. W. Churchill, Journal of Physical Chemistry **59**, 855-863 (1955).
[8] Y. B. Hahn, H. Y. Sohn, Proceedings of a Symposium Mathematical Modeling of Materials Processing Operations, USA, Palm Springs, 799-834 (1987).
[9] C. F. Gerald, P. O. Wheatley, Applied numerical analysis, Addison-Wesley (1994).
[10] J. S. Truelove, Trans. of the ASME **109**, 108-1051 (1987).
[11] W. A. Fiveland, J. of Heat Transfer **106**, 699-706 (1984).
[12] Seung Hyun Kim, Kang, Y. Huh, Int. J. Heat and Mass Transfer **43**, 1233-1242 (2000).
[13] W. A. Fiveland, J. of Heat Transfer **109**, 809-812 (1987).
[14] W. A. Fiveland, J. Thermophys. Heat Transfer **2** (4), 309-316 (1988).
[15] J. S. Truelove, J. Quant, Spectrosc. Radiat. Transfer **39**, 27-31 (1988).
[16] B. Leckner, Combustion and Flame **19**, 33-48 (1972).
[17] C. Crowe, M. Sommerfeld, Y. Tsuji, Multiphase flows with droplets and particles, CRC Press (1998).
[18] A. A. Shook, G. A. Eltringham, B. R. Adams, K. A. Davies, G. Caffery, The Brimacombe memorial symposium, Eds. G. A. Irons, A. W. Cramb, Met. Soc. 349-362 (2001).